HYDRODYNAMIC PERFORMANCE STUDY OF A VERTICAL-AXIS BIO-INSPIRED TIDAL CURRENT TURBINE

Weixing Liu[1,2], Wanting Hu[1], Ziheng Wang[1], Yurii Korol[4], Chengjiao Sun[3*], Haitao Wu[5], Zhihu Yan[2] and Zhiyang Zhang[2,1]

[1] Makarov College of Marine Engineer, Jiangsu Ocean University, Lianyungang, Jiangsu, China

[2] School of Ocean Engineering, Jiangsu Ocean University, Lianyungang, Jiangsu, China

[*3] School of Computer Engineering, Hubei University of Arts and Science, Xiangyang, Hubei, China

[4] Education and Research Center of Hydromechanics, Admiral Makarov National University of Shipbuilding, Mykolaiv, Mykolaiv, Ukraine

[5] Education and Research Center of Hydromechanics, Admiral Makarov National University of Shipbuilding, Mykolaiv, Mykolaiv, Ukraine

[*] Corresponding author; E-mail: jiao1952@126.com

Blades critically influence the energy capture efficiency of tidal flow turbines. In an endeavor to substantially boost the energy performance of tidal current turbines, a vertical-axis bio-inspired blade with a nodular leading edge was designed, based on the humpback whale's pectoral fin, to enhance tidal current turbine performance. The leading edge nodules follow a sine wave pattern. A three-bladed vertical-axis tidal current turbine model incorporating this design was developed. Its hydrodynamic performance was compared to that of a standard three-blade vertical-axis turbine using numerical simulations, with the aim of further and quantifiably improving energy efficiency. The bio-inspired turbine achieved high energy coefficient values. For example, at a tip speed ratio of 2.094, the bio-inspired turbine delivers a 7.12% increase in energy coefficient compared to the standard turbine. Moreover, the bio-inspired turbine demonstrated markedly and consistently higher torque output under low-speed conditions and showcased significantly notable enhanced startup performance.

Key words*: tidal current turbine, bionic blade, humpback whale pectoral fin, hydrodynamic performance, CFD numerical simulation*

1. Introduction

Tidal current energy, a key subset of marine renewable energy, exhibits substantial resource availability, high energy density, and spatial regularity. These characteristics confer significant strategic value and wide-ranging potential for both nearshore and offshore energy development. As the primary component responsible for converting the kinetic energy of seawater into electrical power, the hydraulic performance of tidal turbines directly influences energy conversion efficiency, economic feasibility, and operational reliability. Recent advances in the integration of bionic principles and fluid machinery technologies have introduced novel pathways for the innovative design of tidal turbine blades.

Bionics, grounded in the study of biological systems, informs the engineering design process by replicating structural and dynamic characteristics observed in living organisms [1-3]. By imitating morphological and kinematic traits, bionic approaches address engineering challenges and enhance practical performance [4, 5]. In marine engineering, progressive research into the locomotion of aquatic species such as fish and whales has revealed critical insights into hydrodynamic mechanisms. These developments have facilitated significant advances in bionic technologies, including fish-inspired robots and blades [6, 7]. Considering the success of bionic wind turbine blades, researchers have adapted similar designs for tidal turbines, resulting in various bionic configurations that notably improve power generation efficiency [8, 9].

Batten et al. and Bahaj et al. hypothesized that the design methodologies applied to wind turbine blades could be extended to water turbine blade design [10, 11]. The results confirm that the design theory for wind turbine blades can be applied to the design of horizontal-axis turbine blades and water turbine blades, suggesting key similarities between wind and water turbines. Therefore, these well-established practices in wind turbine design can be employed to optimize the performance and efficiency of water turbines.

Weber et al. revealed that the leading edge of humpback whale pectoral fins in the United States exhibits a distinct nodular structure. Comparative studies demonstrated that blades inspired by this morphology outperformed conventional designs lacking such features, particularly in lift generation and stall delay [12]. These results support the effectiveness of bio-inspired modifications in improving turbine blade performance.

Nedić et al. conducted an experimental study on vortex shedding generated by the serrated trailing edge of an airfoil and evaluated the aerodynamic performance of this configuration [13]. The findings demonstrated that serrations at the trailing edge induce significant vortex shedding, resulting in increased maximum lift and drag coefficients. As a result, the maximum lift-to-drag ratio is reduced compared to that of a conventional airfoil. The study also revealed that the intensity of vortex shedding diminishes as the sawtooth angle decreases.

Rongkang Gao of Ocean University of China investigated the hydrodynamic performance of the black seal shark's fin [14]. A three-dimensional digital model of the fin was developed and used to design a bio-inspired blade for a horizontal-axis hydraulic turbine. Numerical simulations indicated that the bio-inspired blade significantly improves energy efficiency under specific operating conditions, especially at low tip speed ratios. However, this enhancement in performance is accompanied by an increase in axial force, which can introduce pressure distribution instability. Therefore, careful consideration must be given to the trade-off between energy efficiency and potential flow-induced instability during the design and operation of bionic blade turbines.

The present study integrates the distinctive convex nodular structure of the humpback whale pectoral fin into the blade design of a vertical-axis tidal current turbine. This approach draws on the superior hydrodynamic performance of the biological model to overcome the limitations of conventional horizontal-axis bionic turbine designs. A vertical-axis tidal turbine equipped with bio-inspired blades was developed, and its hydrodynamic behavior was analyzed using computational fluid dynamics (CFD) simulations. The results offer a technical reference for the application of bionic blades in vertical-axis tidal current energy systems.

2. Establishment of bionic hydraulic turbine

2.1. Bionic blade design

Humpback whales, among the largest marine mammals, belong to the Baleen family within the order Cetacean Artiodactyla. Because of their specialized feeding mechanisms, these whales exhibit limited overall body flexibility, which restricts their mobility to some extent. However, their flippers are notably longer and more flexible than those of other cetaceans. Miklosovic et al. reported that the leading edges of humpback whale flippers possess a distinct convex nodular structure [15]. These protrusions enhance maneuverability by delaying stall onset, increasing lift, and reducing drag. The pectoral fins of the humpback whale are shown in Fig. 1.

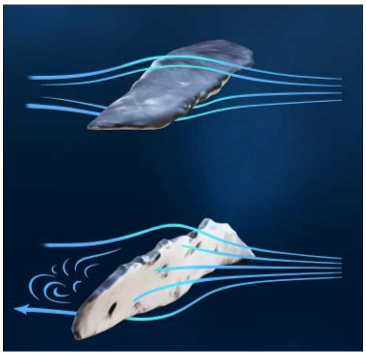

Figure 1 Humpback whale flipper leading edge [16]

Based on the morphological characteristics of the pectoral fin of the humpback whale and the associated hydrodynamic forces, a bionic blade design for a vertical-axis tidal turbine is proposed. In contrast to conventional blades with smooth, straight leading edges, the bionic blades incorporate sinusoidal nodular protrusions. The amplitude of each tubercle is defined as the wave height A, and the length of a single cycle is defined as the wavelength W. According to previous studies, the leading edge of bionic airfoils typically follows a sinusoidal profile [17]. The blade is designed with a chord length c of 100 mm and a span h of 600 mm. A schematic of the pectoral fin of a humpback whale is shown in Fig. 2.

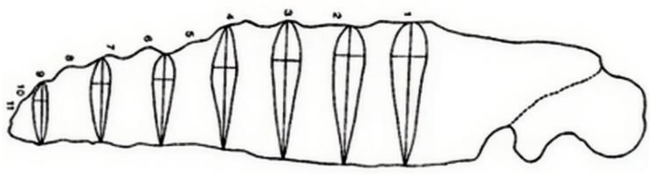

Figure 2 Humpback whale flipper profile [18]

Mehmet Atlar et al. used validated CFD simulations to evaluate the lift characteristics of airfoils with sinusoidal leading-edge tubercles [19]. Results indicated that the optimal aerodynamic performance, reflected in higher lift and lift-to-drag ratios, occurs when the wave height is 0.1 times the chord length. Based on this finding, the present design adopts the same coefficient:

$$A = 0.1c \tag{1}$$

The amplitude of the nodules significantly influences aerodynamic performance, whereas the wavelength has a comparatively minor effect. Cui et al. Cui et al. distributed eight nodules uniformly along the spanwise direction, starting from h = 0 [20]. This configuration yields eight complete sinusoidal cycles along the blade's leading edge, with the wavelength defined as:

$$W = \frac{1}{8}h \tag{2}$$

Accordingly, the bionic blade has a wave height of 10 mm and a wavelength of 75 mm, producing periodic peaks and troughs along its span. These parameters are optimized to emulate the natural flow-enhancing characteristics of the humpback whale flipper. The corresponding equation describing the leading-edge sinusoidal curve in a three-dimensional Cartesian coordinate system is as follows:

$$X = \frac{A}{2}\sin\left(\frac{2Z}{W}\pi - \frac{\pi}{2}\right) + \frac{A}{2} \tag{3}$$

The schematic diagram of the sinusoidal curve of the bionic blade is shown in Figure 3.

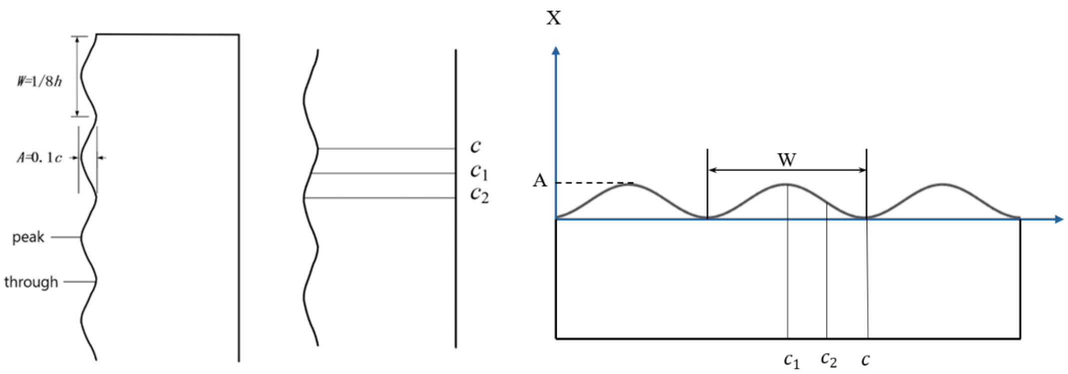

Figure 3 Bionic blade outline schematic cross-section

Previous experimental studies have examined various bionic airfoil geometries by altering the leading-edge profile and airfoil dimensions. Results demonstrated that airfoils designed using nodular leading-edge patterns exhibited superior aerodynamic performance [21]. Based on these findings, the present design adopts the NACA0018 airfoil as the cross-sectional profile for the bionic blade. The nodular structure, composed of crests and troughs, is introduced by proportionally modifying the baseline airfoil geometry to form a sinusoidal leading edge. The chord length and cross-sectional design are expressed by:

$$c_1 = c + A\sin\frac{\pi}{4} \tag{4}$$

$$c_2 = c + A \tag{5}$$

2.2. Bionic turbine establishment

The vertical-axis tidal energy turbine consists primarily of blades, connecting rods, and a rotating shaft. Energy extraction is primarily dependent on the blades. Two hydraulic turbine models were developed: one employing bionic blades and the other standard blades. Both are three-bladed vertical-axis tidal current turbines. The simplified geometries of the bionic and standard turbine models are illustrated in Fig. 4:

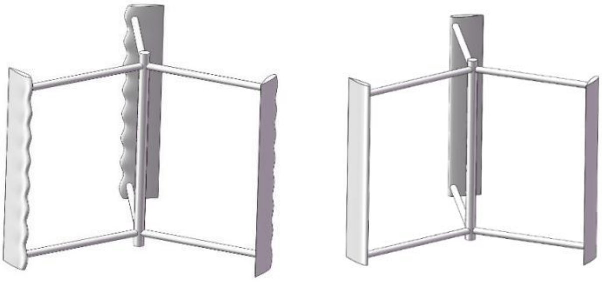

Figure 4 Bionic turbine (left) and standard turbine (right) models

Both models share identical structural parameters, including the number of blades, blade span, blade chord length, and turbine diameter. The main design parameters are listed in Table 1:

Table 1 Main parameters of hydraulic turbine model

Parameter	Parameter value
Number of blades	3
Turbine diameter	1.00m
Rotation axis diameter	0.03m
Blade chord length	0.10m
Blade extension	0.60m
Incoming flow speed	1.50m/s

3. Numerical simulation results and analysis

3.1. Computational domain and meshing

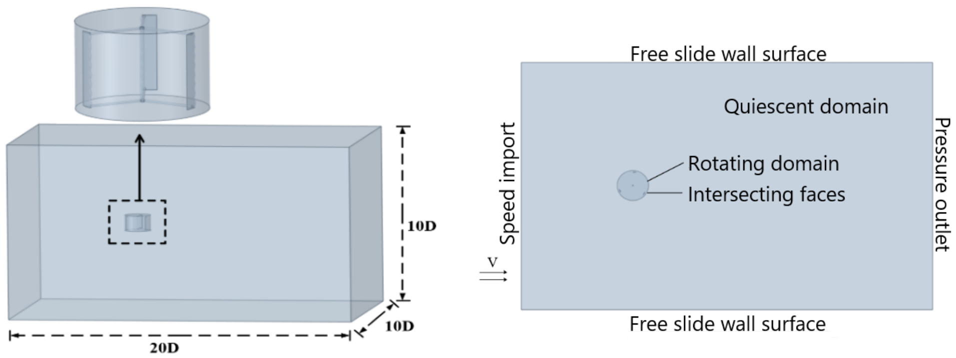

Figure 5 Calculation domain diagram and boundary conditions

The computational domain for both the bionic and standard turbines is a cuboid with dimensions of 20D×10D×10D (where D represents the turbine diameter). The domain is divided into two regions: a static (stationary) domain and a rotating domain. The static domain remains fixed, while the rotating domain allows for the simulation of rotor motion. The center of the rotating domain is positioned 5D from the inlet plane and 15D from the outlet plane, with a 5D distance from each side boundary. The rotating region is modeled as a cylinder with a height of 1.2H and a diameter of 1.2D, as shown in Fig. 5.

The left boundary is defined as a velocity inlet with a constant inflow velocity of 1.5 m/s, assuming uniform flow. The right boundary is set as a pressure outlet with a relative pressure of $P = 0$. The upper, lower, and side boundaries of the static domain are defined as free-slip walls to eliminate wall shear effects and accelerate computation. An interface is specified between the static and rotating regions to ensure continuity in data transfer. The turbine blade surfaces are treated as wall boundaries. For simulations at a tip speed ratio of 2.094, the SST turbulence model is employed, and the solver operates in transient mode. The time step is set to 0.00278 s, corresponding to a 1° rotation per step. The simulation continues until convergence, with a residual threshold of 1×10^{-4}. The torque is monitored throughout the simulation, and the torque curve is obtained after the solution stabilizes. The average torque Q is calculated as follows:

$$Q = \frac{1}{n}\sum_{i=1}^{n} Q_i \tag{6}$$

Where n denotes the number of time steps, and Q_i is the torque value at each time step.

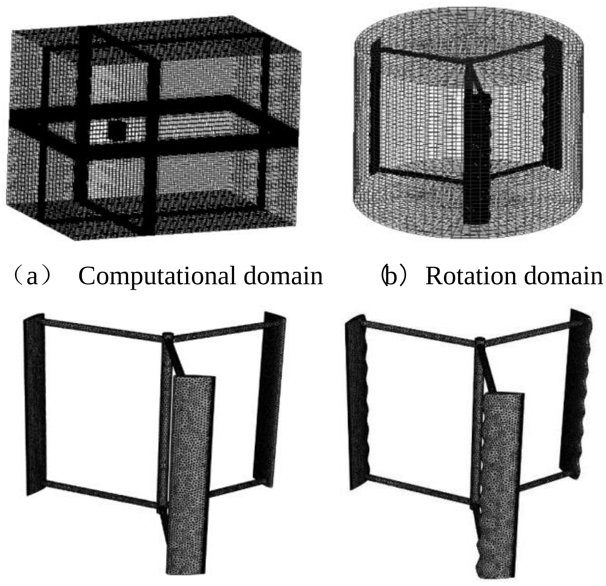

（a） Computational domain （b） Rotation domain

（c） Standard turbine （d） Bionic turbine

Figure 6 Mesh division

In this section, ANSYS ICEM CFD served as the tool for mesh generation. To improve computational efficiency while maintaining accuracy, a hybrid meshing approach is employed, whereby structured grids are used in the computational and rotating domains, while unstructured grids are applied to the turbine model. Mesh refinement is implemented around the turbine blades, where flow behavior is more complex, to enhance resolution and improve result fidelity. In contrast, the mesh in the outer uniform flow field is relatively coarse to reduce computational load. This approach balances simulation accuracy with efficient use of computational resources. In the bionic water turbine, the mesh is locally refined around the three blades. A total of ten prismatic layers is generated along the blade surfaces. The first layer has a thickness of 0.0006 m, with a growth rate of 1.2 per layer, allowing the total thickness of the prism layer region to be calculated. Local mesh refinement around the blades enables accurate capture of flow field variations and ensures computational precision near blade surfaces. The final mesh contains approximately 3.27 million elements for the bionic turbine and 3.02 million elements for the standard turbine. The mesh structure is illustrated in Fig. 6.

3.2. Numerical simulation verification

Before performing full simulations, the accuracy and reliability of the numerical setup were verified to ensure validity while conserving computational time and resources.

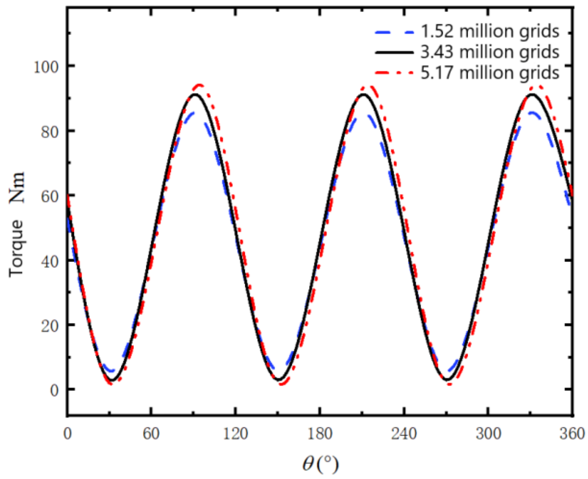

Figure 7 Comparison of torque curves at different meshes

This section uses the vertical-axis single-rotor hydraulic turbine studied by Yang Ransheng at Dalian University of Technology as a validation case [22]. Experimental data showed optimal energy efficiency at an incoming flow velocity of 1.5 m/s. Three grid configurations containing 1.52 million, 3.43 million, and 5.17 million elements were simulated under the same operating conditions: uniform inflow of 1.5 m/s, tip speed ratio of 2.269, and blade attack angle of 0°. Fig. 7 presents torque curve comparisons for these configurations.

Table 2 Grid-independence verification of the standard turbine

	Experimental value	1,520,000 grid	3,430,000 grid	5,170,000 grid
Capacity efficiency	28.6%	27.33%	29.37%	30.58%

Table 2 compares the simulated energy capture coefficients against the experimental reference values. The results show good agreement across all grid sizes. The 1.52-million-grid model slightly underestimates efficiency, while the 3.43-million and 5.17-million grids slightly overestimate it. Among them, the 3.43-million-grid case provides a favorable balance between accuracy and computational efficiency. The relative error across all cases is lower than 10%, which falls within acceptable limits. Furthermore, each torque curve exhibits three distinct peaks and valleys, consistent with experimental observations, confirming the reliability and effectiveness of the numerical simulation methodology.

3.3. Numerical simulation results

3.3.1 Comparison of hydrodynamic performance between bionic turbine and standard turbine

Under uniform flow conditions, the hydrodynamic performance of turbines was analyzed at tip speed ratios of 1.397, 1.745, 2.094, 2.443, and 2.792. Numerical simulations yielded the energy capture coefficient C_{p1} and torque coefficient of the bionic turbine C_{Q1}, while C_{Q2} and C_{p2} correspond to those of the standard turbine.

Table 3 C_{p1}, C_{p2}, C_{Q1} , and C_{Q2} of the turbine

λ	C_{p1}	C_{p2}	C_{Q1}	C_{Q2}
1.397	0.197	0.166	0.141	0.119
1.745	0.278	0.247	0.159	0.141
2.094	0.316	0.295	0.151	0.142
2.443	0.298	0.288	0.122	0.118
2.792	0.271	0.265	0.097	0.095

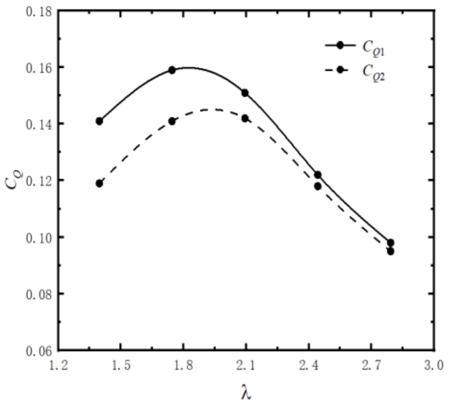

Figure 8 Turbine energy capture coefficient

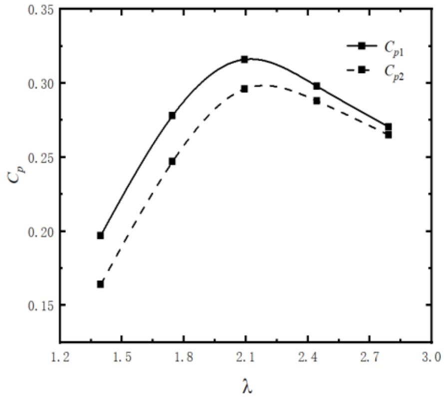

Figure 9 Turbine torque coefficient

Fig. 8 shows that the energy capture coefficient for both turbines increases initially with the tip speed ratio, reaching a peak at 2.094, followed by a decline. At this peak, the bionic turbine's energy capture coefficient exceeds that of the standard turbine by 7.12%. When the tip speed ratio is lower than 2.094, the bionic turbine demonstrates substantial energy efficiency improvements, with an 18.67% increase at 1.397. When the tip speed ratio is higher than 2.094, the energy capture coefficient of the bionic turbine is slightly reduced, but the decline remains minimal.

Torque primarily arises from the pressure moment exerted by the water flow on the blades, closely linking the torque coefficient to energy harvesting efficiency. Fig. 9 shows that for the standard turbine, the torque coefficient increases up to 2.094 and decreases beyond this value. By contrast, the bionic turbine's torque coefficient increases until 1.745, then decreases at higher tip speed ratios. At tip speed ratios exceeding 2.094, the flow velocity becomes sufficiently high for inertial forces to dominate flow-blade interactions. Under these conditions, the influence of blade shape diminishes, and the flow behaves as a high-speed jet impacting the blades. Both turbine models exhibit similar torque generation mechanisms and energy conversion at this stage. However, the bionic turbine generates higher torque at lower speeds, facilitating easier startup compared to the standard turbine.

3.3.2 Torque analysis

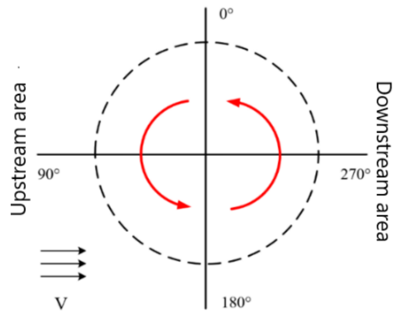

Figure 10 Azimuthal division

The azimuth angle of the turbine during rotation is defined as follows: The turbine rotates counterclockwise under uniform flow from left to right. The region with an azimuth angle of 90° ± 90° corresponds to the upstream area, while the region at 270° ± 90° corresponds to the downstream area (Fig. 10).

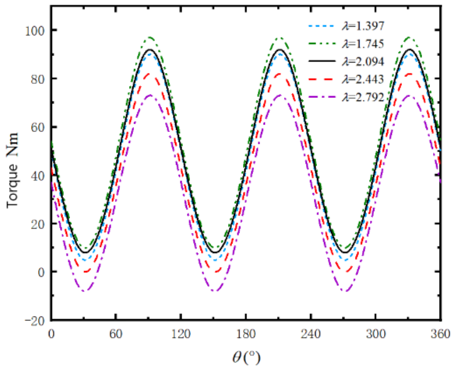

Figure 11 Bionic turbine single cycle torque

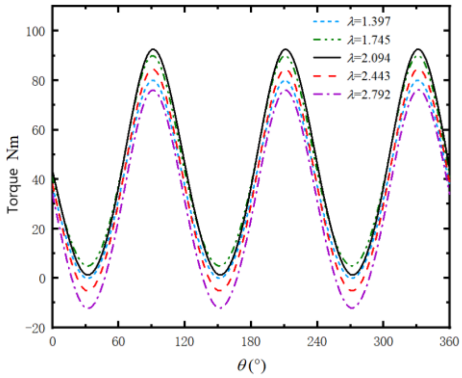

Figure 12 Standard turbine single cycle torque

Table 4 Bionic turbine and standard turbine torque

	λ=1.397	λ=1.745	λ=2.094	λ=2.443	λ=2.792
Q_1 (Nm)	47.532	53.660	50.829	41.086	32.565
Q_2 (Nm)	40.063	47.676	47.451	39.708	31.962

Figs. 11 and 12 show the torque variation during a single rotation cycle for the bionic and standard turbines, respectively. The turbine torque exhibits a stable periodic pattern with three peaks and three valleys per cycle. Torque magnitude varies across different tip speed ratios. Table 4 presents the torque values for both turbines at varying tip speed ratios. Q_1 represents the torque of the bionic turbine, and Q_2 represents the torque of the standard turbine. Both turbines reach their maximum torque at a tip speed ratio of 1.745. At this ratio, Q_1 exceeds Q_2 by 12.55%.

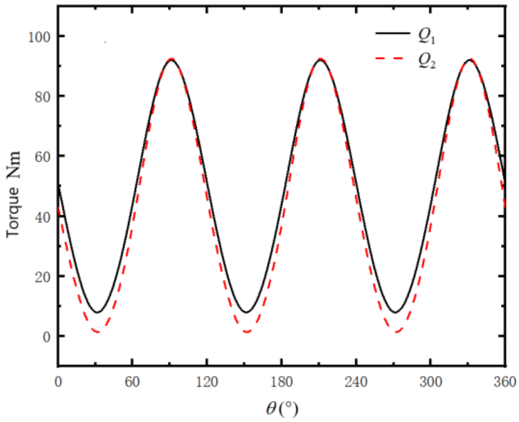

Figure 13 Torque curves of bionic turbine and standard turbine

The blades exhibit varying energy outputs at different positions. Consequently, the water flow energy received by the turbine at different azimuths is unevenly distributed, resulting in periodic fluctuations in torque. When the flow velocity is 1.5 m/s and the tip speed ratio is 2.094, both the bionic and standard turbines reach their maximum energy acquisition coefficient. Fig. 13 compares the torque curves of the bionic and standard turbines under these conditions. The torque peaks occur near azimuth angles of 90° , 210° , and 330° , while the minima are observed near 30° , 150° , and 270° . Under these conditions, the peak torque for both turbines stabilizes around 93 Nm. However, the valley torque values of the bionic turbine are higher than those of the standard turbine.

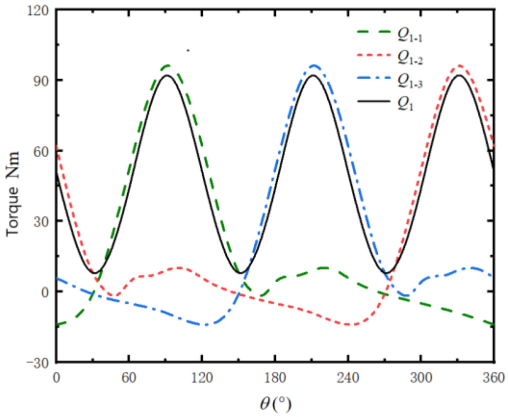

Figure14 Torque of three blades in the bionic turbine

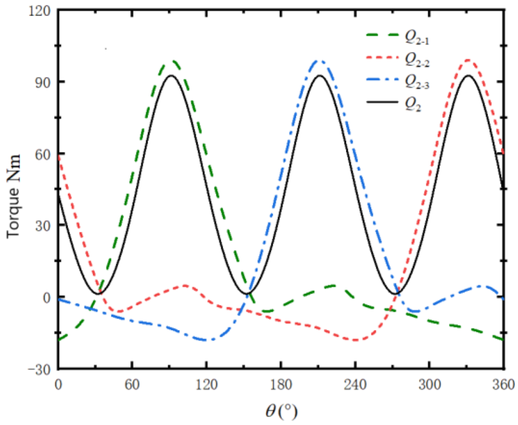

Figure 15 Torque of three blades in the standard turbine

The three blades of the bionic and standard turbines at azimuths of 0°, 120°, and 240° are labeled as 1-1, 1-2, 1-3 and 2-1, 2-2, 2-3, respectively. The total turbine torque is the sum of the torques from all three blades at each azimuthal position. As shown in Figs. 14 and 15, each blade produces a torque peak once per rotation, typically near the 90° azimuth, when the blade is located in the upstream region (90° ± 90°). In this region, the flow velocity is higher and the flow field is more stable. The stronger hydrodynamic force acting on the blade provides more kinetic energy, enhancing blade performance. As a result, the blade generates higher torque in this region. By contrast, when the blade moves into the downstream region (270° ± 90°), wake vortex shedding behind the blade reduces the local flow velocity. This limits energy transfer, causing the blade torque to drop significantly, and in some cases, even become negative. Figs. 14 and 15 show that the torque values of the bionic turbine blades in the downstream region are consistently higher than those of the standard turbine blades, resulting in a greater total torque for the bionic turbine.

4. Flow field analysis

The torque coefficient and energy capture coefficient depend directly on the pressure and flow field characteristics during turbine operation. This section analyzes the pressure distribution and flow field characteristics of the bionic and standard turbines at azimuth angles of 0°, 30°, 60°, and 90°, under an incoming flow velocity of 1.5 m/s and a tip speed ratio of 2.094.

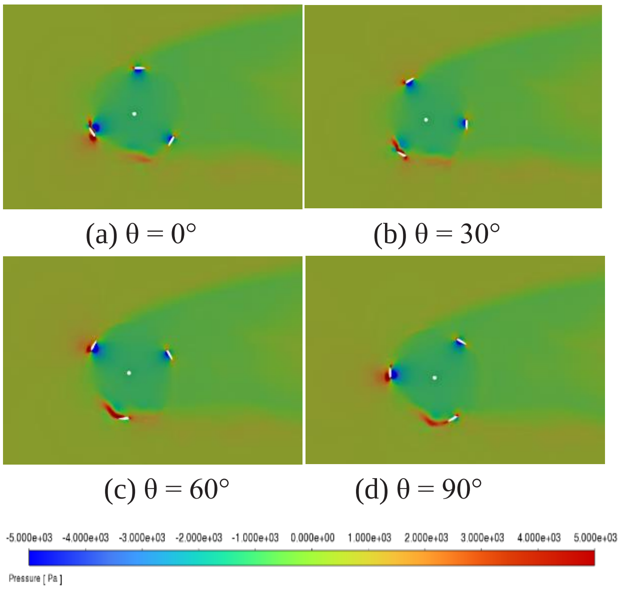

(a) θ = 0° (b) θ = 30°

(c) θ = 60° (d) θ = 90°

Figure 16 Bionic turbine pressure cloud

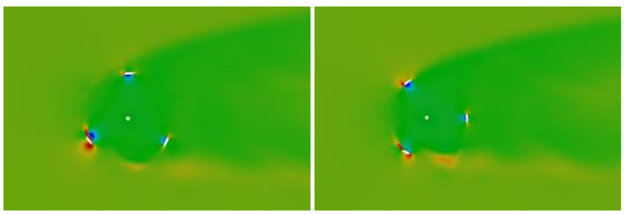

(a) θ = 0° (b) θ = 30°

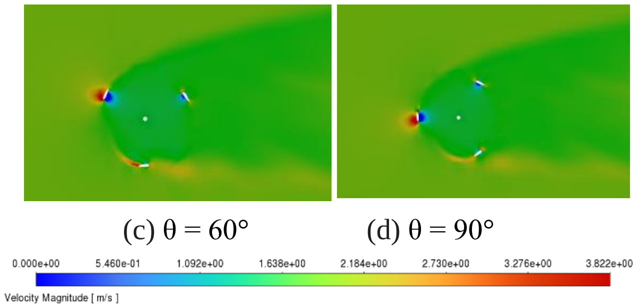

Figure 17 Standard turbine pressure cloud

Figs. 16 and 17 present the pressure cloud diagrams of the bionic and standard hydraulic turbines, respectively. The pressure in the upstream region is higher than in the downstream region. As water flows through the turbine, a wake field forms behind it, leading to a pressure drop in the downstream area. Within the azimuth range of 0°–90°, the pressure at the blade’s leading edge gradually increases and exceeds that at the trailing edge. At 90°, the leading edge pressure reaches its maximum. At this position, the blade is on the upstream side, where the pressure differential between the inner and outer surfaces of the blade is at its maximum, resulting in peak torque. From 90° to 180°, the leading edge pressure gradually decreases, while the trailing edge pressure increases. This pressure change forms a long and narrow wake behind the blade. At 180°, the pressure difference between the blade's inner and outer surfaces is roughly 0. In the upstream region, the pressure distribution of the bionic turbine closely resembles that of the standard turbine. From 180° to 270°, the pressure difference between the inner and outer surfaces of a single blade is small, and the torque generated is correspondingly low. However, in this region, the pressure differential across the blade of the bionic turbine exceeds that of the standard turbine, resulting in greater torque output. In the 270°–360° azimuth range, a negative pressure zone appears near the trailing edge of the single blade, causing a sharp drop in pressure and torque for both turbine types. These results indicate that the turbine generates more work in the upstream region than in the downstream region.

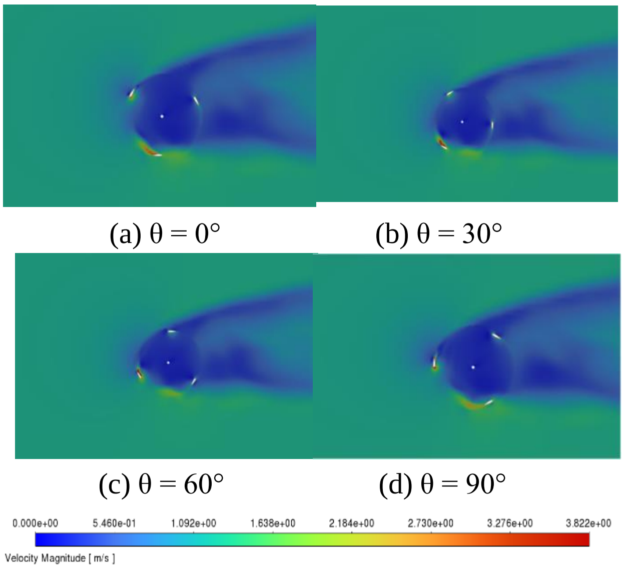

Figure 18 Velocity cloud of bionic turbine

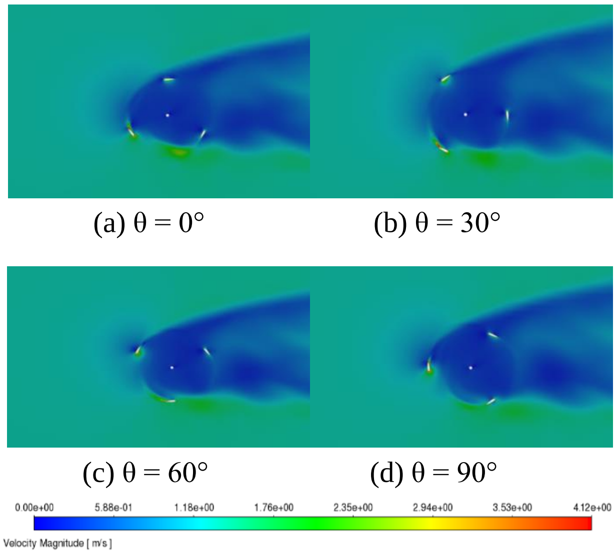

Figure 19 Velocity cloud of standard turbine

Figs. 18 and 19 display the velocity cloud diagrams of the bionic and standard turbines. The velocity in the upstream region is markedly higher than in the downstream region. As the turbine extracts energy from the water flow, the flow velocity within the turbine decreases significantly, and a low-speed wake is generated downstream. Both turbines exhibit similar upstream flow field characteristics. A localized high-speed zone develops near the blade surfaces. Between 0° and 90°, the velocity at the blade's leading edge gradually increases. After 90°, the high-speed zone begins to shift toward the trailing edge. From 90° to 270°, the flow velocity at the trailing edge increases, with the bionic turbine maintaining higher velocities than the standard turbine. From 270° to 360°, the trailing edge velocity decreases as the high-speed zone at the leading edge diminishes.

Figs. 18 and 19 correspond to operating conditions at $\lambda = 2.094$. At this tip speed ratio, inertial forces dominate over viscous forces, and the "microscale" disturbances caused by the bionic nodules are masked by the high-speed mainstream. As a result, the velocity fields of the two turbines converge toward a similar flow pattern, further confirming that performance differences diminish when $\lambda > 2.094$. The downstream wake of the standard turbine (Figs. 19c and 19d) is broader, indicating greater energy loss. In contrast, the bionic turbine generates a narrower low-speed wake, particularly between 180° and 270°, suggesting reduced flow energy dissipation.

5. Conclusions

A three-blade vertical axis tidal current bionic turbine was designed and analyzed using CFD numerical simulation. Its hydrodynamic performance was compared with a standard turbine. Energy aQuisition coefficients and torque coefficients were simulated under varying tip speed ratios. Torque curves and flow field characteristics during turbine rotation were examined. The main conclusions are as follows:

(i) The bionic turbine achieved a high energy harvesting coefficient, peaking at $\lambda = 2.094$. At this tip speed ratio, the bionic turbine's energy harvesting coefficient exceeded that of the standard turbine by 7.12%. When $\lambda < 2.094$, the bionic turbine showed significant improvement in energy harvesting efficiency. Beyond this value, the increase in energy harvesting coefficient was marginal.

(ii) The torque coefficient of the bionic turbine exceeded that of the standard turbine. At λ = 1.745, the torque exceeded the standard turbine's by 12.55%. The bionic turbine generated greater torque at low speeds, facilitating easier startup. Additionally, torque attenuation in the downstream region (270° ± 90°) was smaller for the bionic blade, indicating stronger wake energy recovery and enhanced low-speed starting performance.

The simulation scope was limited to tip speed ratios λ = 1.397 to 2.792 and an inflow velocity of 1.5 m/s. Extreme flow velocities (> 3 m/s), variable flow conditions (e.g., turbulence, shear flow), and multi-unit array effects were not considered. The turbine's adaptability to complex marine environments requires further verification. Future work will extend simulations to lower flow velocities, higher turbulence intensities, and dynamic tip speed ratio processes. This will enable assessment of energy capture under unsteady flow conditions typical of tidal energy.

Acknowledgment

The authors Weixing Liu, Zhiyang Zhang, and Haitao Wu contributed equally to the completion of this study. Financial support was provided by the National Natural Science Foundation of China (Nos. 52101356, 52471284), Natural Science Foundation of Hubei Province (2024AFB147), Lianyungang Sixth "521 Project" Research Project Funding Program (No. LYG065212024049), and the 2024 Jiangsu Province Qinglan Project for Outstanding Young Backbone Teachers.

References

[1] Yang, Z., & Tong, Z. Bio-inspired design for impeller and diffuser optimization to enhance the hydraulic performance of slanted axial flow pumps. *Physics of Fluids*, 2024, *36*(12). https://doi.org/10.1063/5.0244902

[2] Nachtigall, W., & Wisser, A. *Bionics by examples*. Heidelberg: springer, 2014 https://doi.org/10.1007/978-3-319-05858-0

[3] Wang, J., Chen, L., Tan, Z., Du, E., Liu, N., Ma, J., ... & He, G. Inherent spatiotemporal uncertainty of renewable power in China. *Nature Communications*, 2023, *14*(1), 5379. https://doi.org/10.1038/s41467-023-40670-7

[4] Wang, X., Yang, J. F., Huang, X. W., & Wang, W. Q. Using bionic tubercles to control swirling flow instabilities of a hydraulic turbine during the load rejection process. *Energy*, 2024, *311*, 133354. https://doi.org/10.1016/j.energy.2024.133354

[5] Tian, G., Fan, D., Feng, X., & Zhou, H. Thriving artificial underwater drag-reduction materials inspired from aquatic animals: progresses and challenges. *RSC advances*, 2021, *11*(6), 3399-3428. https://doi.org/10.1039/D0RA08672J

[6] Lei, H., Zhou, D., Bao, Y., Chen, C., Ma, N., & Han, Z. Numerical simulations of the unsteady aerodynamics of a floating vertical axis wind turbine in surge motion. *Energy*, 2017, *127*, 1-17. https://doi.org/10.1016/j.energy.2017.03.087

[7] Luo, K., Yan, L., Zhu, Z., Wang, Z., Wang, H., & Jiang, F. Application of Bionic Technology in Marine Cruise Equipment: Research Progress and Development Trends. *Journal of Bionic Engineering*, 2024, *21*(3), 1117-1155. https://doi.org/10.1007/s42235-024-00483-w

[8] Kulkarni, S., Chapman, C., Shah, H., Parn, E. A., & Edwards, D. J. Designing an efficient tidal turbine blade through bio-mimicry: A systematic review. *Journal of Engineering, Design and Technology*, 2018, *16*(1), 101-124. https://doi.org/10.1108/JEDT-08-2017-0077

[9] Zhang, K., Yang, S., Gao, Z., & Zhang, B. (2021). The blade design of a bionic shark fin airfoil for a horizontal axis tidal current turbine. *Journal of Energy Engineering*, 2021, *147*(6), 04021054. https://doi.org/10.1061/(ASCE)EY.1943-7897.0000807

[10] Batten, W. M. J., Bahaj, A. S., Molland, A. F., Chaplin, J. R., & Sustainable Energy Research Group. Experimentally validated numerical method for the hydrodynamic design of horizontal axis tidal turbines. *Ocean engineering*, 2007, *34*(7), 1013-1020. https://doi.org/10.1016/j.oceaneng.2006.04.008

[11] Bahaj, A. S., Batten, W. M. J., & McCann, G. Experimental verifications of numerical predictions for the hydrodynamic performance of horizontal axis marine current turbines. *Renewable energy*, 2007, *32*(15), 2479-2490. https://doi.org/10.1016/j.renene.2007.10.001

[12] Weber, P. W., Howle, L. E., Murray, M. M., & Fish, F. E. Lift and drag performance of odontocete cetacean flippers. *Journal of Experimental Biology*, 2009, *212*(14), 2149-2158. https://doi.org/10.1242/jeb.029868

[13] Nedić, J., & Vassilicos, J. C. Vortex shedding and aerodynamic performance of airfoil with multiscale trailing-edge modifications. *AIAA Journal*, 2015, *53*(11), 3240-3250. https://doi.org/10.2514/1.J053834

[14] R. Gao. Research on bionic blades of horizontal axis tidal current turbine based on shark fin (in Chinese), Ph. D. thesis, Ocean University of China, Qingdao, China, 2014.

[15] Miklosovic, D. S., Murray, M. M., Howle, L. E., & Fish, F. E. Leading-edge tubercles delay stall on humpback whale (Megaptera novaeangliae) flippers. *Physics of Fluids*, 2004, *16*(5), L39–L42. https://doi.org/10.1063/1.1688341

[16] Kosma MM, Werth AJ, Szabo AR, Straley JM. Pectoral herding: an innovative tactic for humpback whale foraging. *Royal Society Open Science*, 2019, *6*(10): 191104. http://dx.doi.org/10.1098/rsos.191104

[17] Shi, W., Rosli, R., Atlar, M., Norman, R., Wang, D., & Yang, W. Hydrodynamic performance evaluation of a tidal turbine with leading-edge tubercles. *Ocean Engineering*, 2016, *117*, 246-253. https://doi.org/10.1016/j.oceaneng.2016.03.044

[18] Fish, F. E., & Battle, J. M. Hydrodynamic design of the humpback whale flipper. *Journal of morphology*, 1995, *225*(1), 51-60. https://doi.org/10.1002/jmor.1052250105

[19] Atlar Mehmet. Numerical Simulation of a Tidal Turbine Based Hydrofoil with Leading-Edge Tubercles. *International Conference on Offshore Mechanics and Arctic Engineering*. American Society of Mechanical Engineers (Vol. 49972, p. V006T09A005), American Society of Mechanical Engineers, 2016. doi:10.1115/OMAE2016-54796

[20] Cui, Y., Xu, D., Liu, Z., & Ross, D. Global Research and Trends in Renewable Energy: Ocean Waves, Tidal Energy and Offshore Wind. *Journal of Coastal Research*, 2020, *95*(SI), 1485-1489. https://doi.org/10.2112/SI95-286.1

[21] Johari, H., Henoch, C., Custodio, D., & Levshin, A. Effects of leading-edge protuberances on airfoil performance. *AIAA journal*, 2007, *45*(11), 2634-2642. https://doi.org/10.2514/1.28497

[22] R. Yang, Experimental and numerical study of hydrodynamic performance of vertical axis tidal turbine (in Chinese), Ph. D. thesis, Dalian University of Technology, Dalian, China, 2013.

Submitted: 12.07.2025
Revised: 05.09.2025
Accepted: 16.09.2025